FORUM GEOGRAFI
ISSN: 0852-0682 | E-ISSN: 2460-3945
HTTPS://JOURNALS.UMS.AC.ID/INDEX.PHP/FG/

*Research article*

# Monitoring Lake Water Temperature and Estimating Evaporation in Western Iraq Using Ground-based Meteorological Observations and Satellite Remote Sensing

**Abdulqader Mahdi Salh[1,*], Bilal Bardan Ali[2], Ahmed M. El Kenawy[3], Khamis Daham Muslih[4], Sara Ismail Chiad[5]**

[1] Higher Institute of Desert Sciences, University of Anbar, Ramadi, 31001, Iraq; [2] Department of Geography, College of Education for Humanities, University of Anbar, Anbar, Iraq; [3] Instituto Pirenaico de Ecologia, Campus de Aula Dei, 1005, 50059, Zaragoza, Spain; Department of Geography, Mansoura University, Mansoura, 35516, Egypt; [4] University of Baghdad, College of Arts, Department of Geography & GIS; [5] Higher Institute of Desert Sciences, University of Anbar, Ramadi, 31001, Iraq.

[*)] Correspondence: abdulqader.mahdi@uoanbar.edu.iq

**Citation:**
Salh, A. M., Ali, B. B., El Kenawy, A. M., Muslih, K. d., & Chiad, S. I. (2026). Monitoring Lake Water Temperatures and Estimating Evaporation in Western Iraq Using Ground-based Observations and Satellite Remote Sensing. Forum Geografi. 41(1), 72-90.

**Article history:**
Received: 30 May 2026
Revised: 06 September 2026
Accepted: 06 September 2026
Published: 14 September 2026

## Abstract

Monitoring and estimating water loss rates from lakes in arid regions is challenging due to the scarcity of climate data. Therefore, this study aimed to investigate the spatiotemporal variation of lake surface temperature and evaporation for Tharthar Lake (western Iraq) using ground meteorological observations and satellite remote sensing technique. Three meteorological parameters—air temperature, humidity, and wind—were used in this study to conduct temporal analysis from January–December 2023. These parameters are available in the dataset of Tikrit weather station. Land Surface Temperature (LST) was obtained by processing thermal and infrared data of Landsat 9. Further, evaporation was calculated by the METRIC (Mapping Evapotranspiration at High Resolution with Internalized Calibration) model by solving the surface energy balance and scaling the instantaneous surface fluxes to daily and seasonal totals. The METRIC model was validated by an independent machine learning-based validation. The results demonstrate that the temperature of the air in contact with the lake surface varies seasonally, ranging between 3.2 °C (January) and 47 °C (July). Additionally, relative humidity displays a seasonal pattern: declining from approximately 79% (winter) to 19% (summer). Evaporation during winter and summer was less than 1 mm /day and over 4 mm /day, respectively. The evaporation rate exhibited a clear spatial discontinuity where the evaporation loss was relatively higher along the shallow periphery and southern parts of the lake compared to the deep central areas. Evaporation dynamics and seasonal variation of the lake are primarily governed by atmospheric forces. Notably, the evident seasonal evaporation indicates that Tharthar Lake is vulnerable to considerable seasonal water loss. The approach used in this study is a flexible method for evaporation monitoring at lakes in arid and data-scarce regions and can be applied in Iraq, where similar conditions are prevalent, to support the sustainable management of water resources.

Keywords: Evaporation Estimation; Tharthar Lake; METRIC Model; Band 10 Data; Landsat Satellite.

## 1. Introduction

Lakes found in semi-arid and arid regions are crucial to the sustenance of water resources and local climate regulation, along with the facilitation of ecological processes. In addition to being reservoirs for domestic and agricultural purposes, lakes are vital and sensitive evaluators of environmental and climate changes (Lyons & Shengm, 2017; Bai & Wang, 2023). Currently, these systems are threatened by climate change and human activities, including reduced precipitation, rising temperatures, salinization, pollution, and land-use shifts. All of these likely accelerate the deterioration of ecosystems and scarcity of water (Laounia *et al*., 2017; Chávez *et al*., 2009). In arid basins, artificial recharge, diversions, and flood control implemented as management interventions further alter hydrological systems, thereby leading to complex trade-offs for availability of water and ecosystem services as well as the ability of these systems to sustain themselves in the long term (Chen *et al*., 2025; Zhang *et al*., 2024).

The impact of climate change, coupled with increased desertification and hydrological instability, can turn once permanent lakes into seasonal or even ephemeral ones (Huang *et al*., 2022; Alsumaiei *et al*., 2025). Human activities such as the construction of upstream dams and withdrawals for irrigation have resulted in worldwide shrinkage of major inland water bodies (Oroud, 2019). Salinization has further deteriorated water quality and aquatic ecosystems, and directly impacted biodiversity, water security, agriculture, and the regional economy. (Bastiaanssen *et al*., 1998; Wang *et al*., 2015). The combined effects of climate change and human activities on these water bodies have increased the need to monitor lakes in arid and semi-arid regions and to develop effective management strategies.

Lake surface temperature (LST) influences both its physical and ecological aspects by governing the vertical and horizontal distribution of water in the lake, its biological productivity, and even

CC BY

**Copyright:** © 2027 by the authors. Submitted for possible open access publication under the terms and conditions of the Creative Commons Attribution (CC BY) license (https://creativecommons.org/licenses/by/4.0/).

the rate of water loss through evaporation (Abir *et al*., 2024; Utami, & Kim, 2023). Previous investigations have revealed that the surface of lakes, especially shallow lakes, experience more rapid warming than the air temperature, which consequently enhances the evaporation rates of lakes in regions with prolonged drought (Woolway *et al*., 2018; Zhou *et al*., 2021). In these areas, evaporation is typically the primary mechanism of water loss from the lake, and is often greater than the total annual precipitation, thereby leading to considerable reductions in lake volume (Li *et al*., 2009; Lima *et al*., 2020). Recent studies have indicated that mechanisms of water loss are likely to vary as one moves between different dryland areas. This indicates the importance of evaluating the surface temperature and evaporation patterns of lakes accurately (Maleki *et al*., 2024).

These challenges are particularly evident in western Iraq, which has an arid to semi-arid climate characterized by low precipitation and high evaporation (Al-Daghistani, 2003; Ali *et al*., 2021). Over the years, this region has experienced increased temperatures coupled with decreased precipitation which has resulted in lower river flow and severe drought and water stress (Micijevic *et al*., 2019). Furthermore, restrictions placed on the flow of the Tigris and Euphrates rivers, along with climate change, have created additional challenges for lakes and reservoirs that are critical to sustain irrigation, flood control, and ecosystem services (Sharma *et al*., 2024; Singh *et al*., 2024). Notably, remote sensing studies demonstrate that the surface area and storage volume of many Iraqi lakes are shrinking, thus, illustrating the extreme impacts of climate change and anthropogenic impacts (Ahmood *et al*., 2024; Holman *et al*., 2023).

In Iraq, satellite-based remote sensing has significantly contributed to the temporal and spatial monitoring of inland water bodies. However, previous hydrological studies of Lake Tharthar have primarily focused on surface area dynamics and volumetric fluctuations (Forootan, 2019; Fadel & Najiban, 2024). Although some recent attempts have attempted to estimate evaporation rates using remote sensing (Forootan, 2019; Biggs *et al*., 2016). these studies have largely relied on simplified empirical equations, low-resolution climate networks, or general land-temperature products without accurate correlation to actual water surface temperatures (Ahmood *et al*., 2024). Consequently, the lack of continuous and high-resolution integration between satellite-derived lake surface temperatures and local terrestrial climate observations of Lake Tharthar remains a critical research gap (Matta *et al*., 2022).

To bridge this gap, to the best of our knowledge, this study is the first to develop a precise and highly decomposed framework that integrates multi-source thermal remote sensing with local terrestrial meteorological data. This approach directly adapts to microclimatic feedback and the thermal hysteresis of Lake Tharthar, thereby providing more dynamic and accurate evaporation estimates compared to previous evaporation models.

This study aimed to analyze the surface temperature of Tharthar Lake in the west of Iraq and discover the spatiotemporal evaporation. Landsat 9 thermal datasets and ground-based data were used to obtain this data. Subsequently, the METRIC surface energy balance model was adopted for further investigation. This model enabled evaluation of the lake surface evaporation by constructing a physically based evaporation model. Furthermore, it verified the satellite data of evaporation by using machine learning-based validation. This offered valuable insight into future evaporation trends in relation to the management of the data-poor and climate-affected national water resources. Importantly, this study creates a framework that can be adopted for measuring lake evaporation in dry climates worldwide.

## 2. Methods

Figure 1 illustrates the overall methodological framework used to estimate and evaluate lake evaporation using an internally calibrated surface energy balance model. The first stage of the methodology involves the acquisition and preprocessing of three primary data sources: Landsat 9 satellite data, specifically the optical bands of the OLI-2 sensor and the thermal band 10 of the TIRS-2 sensor, spatially adjusted to a resolution of 30 meters. Hourly climate readings from the Tikrit ground station, including downward solar radiation, air temperature, relative humidity, and wind speed, are also utilized, coupled with historical records of basin evaporation and climate data obtained from the Tikrit station for evaluation and validation purposes.

To ensure that the open water area is evaluated exclusively, without influence from the adjacent land, a dynamic water mask was constructed based on the Modified Water Differences Index (MNDWI) with a threshold value exceeding 0.10, combined with a Quality of Data (QA_PIXEL) band to mask clouds and shadows. Thereafter, atmospheric correction of the spectral radiation recorded in the thermal band was performed using radiative transport data based on the MODTRAN model and NCEP reanalysis data. A constant emissivity of 0.990 for pure water was assigned to derive the surface temperature of the lake via Planck's inversion.

The next stage of the methodology involved calculating the fundamental components of the surface energy budget, namely latent evaporation. Net radiation was calculated based on a hydroalpido-coefficient between 0.05 and 0.06. To facilitate the handling of the high heat capacity of water, hydrothermal flux was calculated as a dynamically variable ratio of net radiation between 0.30 and 0.50. Further, aerodynamic impedance was designed to calculate the perceived heat flux, while assuming an open-water momentum angle roughness coefficient of 0.0003 m.

This study employed an internal calibration technique by establishing two reference points in each spatial snapshot to automatically eliminate thermal and atmospheric biases. The first sample comprised a "cold pixel" taken in deep, clear water areas where perceptible heat flow was almost nonexistent and evaporation is at its maximum. The second sample consisted of a "hot pixel" collected in the dry, bare land surrounding the lake where evaporation was negligible. This enabled the extraction of linear temperature gradient features and supported the model calculations.

During the temporal scaling phase, the instantaneous evaporation ratio was calculated relative to the reference evaporation, which was estimated using the standard Penman-Monteath equation (ASCE). Assuming that this ratio is stable throughout the hours of the day, the calculations were extended to extract the total daily evaporation of the lake in millimeters per day. The methodology concluded with an uncertainty and conformity assessment, in which 80% of the data were used for training while the remaining 20% for testing, with accuracy evaluated using artificial intelligence algorithms (EEDNN, Random Forest, SAM, and LGBM) based on the statistical measures of mean squared error (MSE), root mean squared error (RMSE), and Nash-Soutcliffe efficiency (NSE).

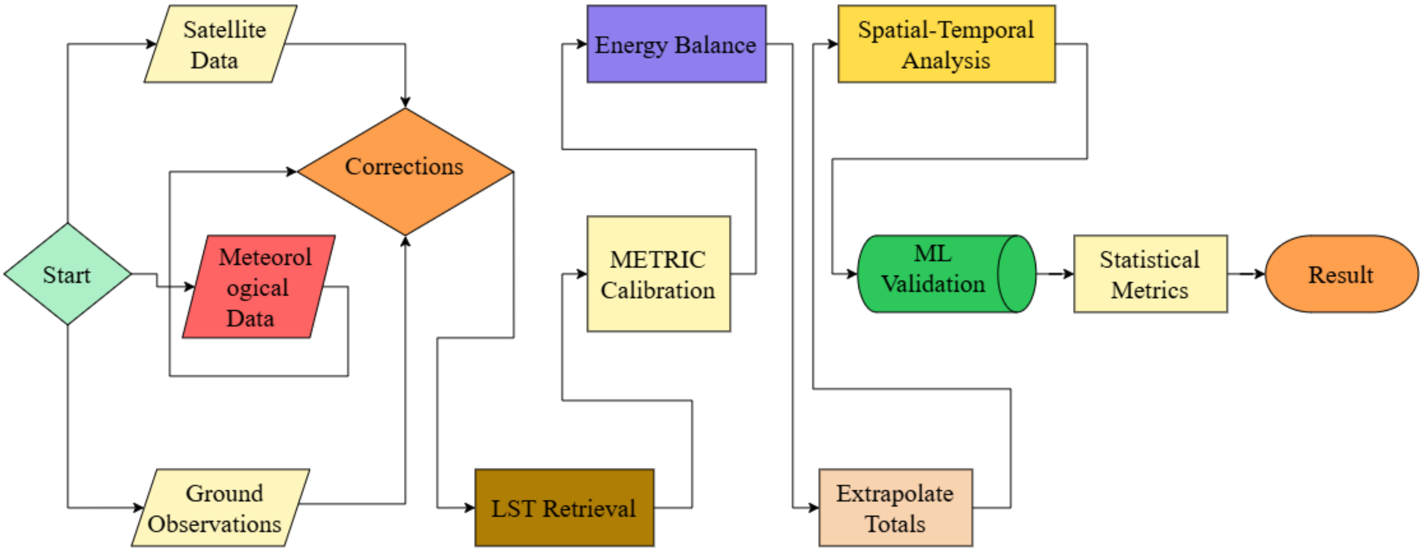


**Figure 1.** A flowchart for Processing Climate and Space Data, Calibrating the METRIC Model, and Verifying Results Using Machine Learning.

## 2.1. Study Area

Lake Tharthar, located between the Tigris and Euphrates rivers, is the largest natural depression in Iraq, situated approximately 120 km northwest of Baghdad (Figure 2). The basin extends across the Salah al-Din and Al-Anbar governorates and is positioned between latitudes 33°39′–34°50′ N and longitudes 42°57′–43°40′ E; its central coordinates are approximately 33.97° N and 43.18° E. The depression, which is approximately 120 km in length and up to 48 km in width, was primarily formed through karst processes within the Miocene gypsum of the Fatha Formation and has been modified by subsidence (Hussain, 2024). Al-Obaidi (2009) estimates that the lake occupies approximately 2,710 km² when it is operating at full capacity.

Lake Tharthar serves as a managed reservoir within the Iraqi flood-control system. The minimum operational level of 40 m corresponds to a storage capacity of approximately 35.18 billion m³, while the maximum operating level of 65 m above sea level permits the storage of up to 85.59 billion m³ of water (Hussain, 2024). Additionally, the hydrological regime of the lake is highly variable due to the arid to semi-arid climate of the region. The annual rainfall is typically less than

200 mm, while the evaporation rate exceeds 1.9 m yr⁻¹ (Fadel & Najiban, 2024). Recent evaluations suggest that water storage has substantially decreased, with the lake volume having shrunk to nearly 40% of its capacity by 2023, with this change primarily attributed to climatic variability (Hussain, 2024).

Evaporation is a significant factor in the water balance of the lake, with an estimated annual loss of approximately 2.93 billion m³ under current conditions and a potential increase to over 5.08 billion m³ at full storage capacity (Fadel & Najiban, 2024). Additionally, the volume and surface area of lakes change dynamically over extended droughts, accompanied by increases in salinity. Remote sensing reports large scale shoreline retreat (444 km² between 1990 and 2003) indicating the high sensitivity of the lake to hydrological and climatic factors (Ahmood *et al*., 2024).

Lake Tharthar is located in the center of the steppe in Iraq, and its hydrological importance is complemented by its ecological significance as a seasonal wetland. Lake Tharthar sustains a variety of habitats and demonstrates highly flexible water levels (Abdullah *et al*., 2019). Through the interplay of hydrological and ecological factors, Lake Tharthar is one of the most significant geographic and environmental features in western Iraq.

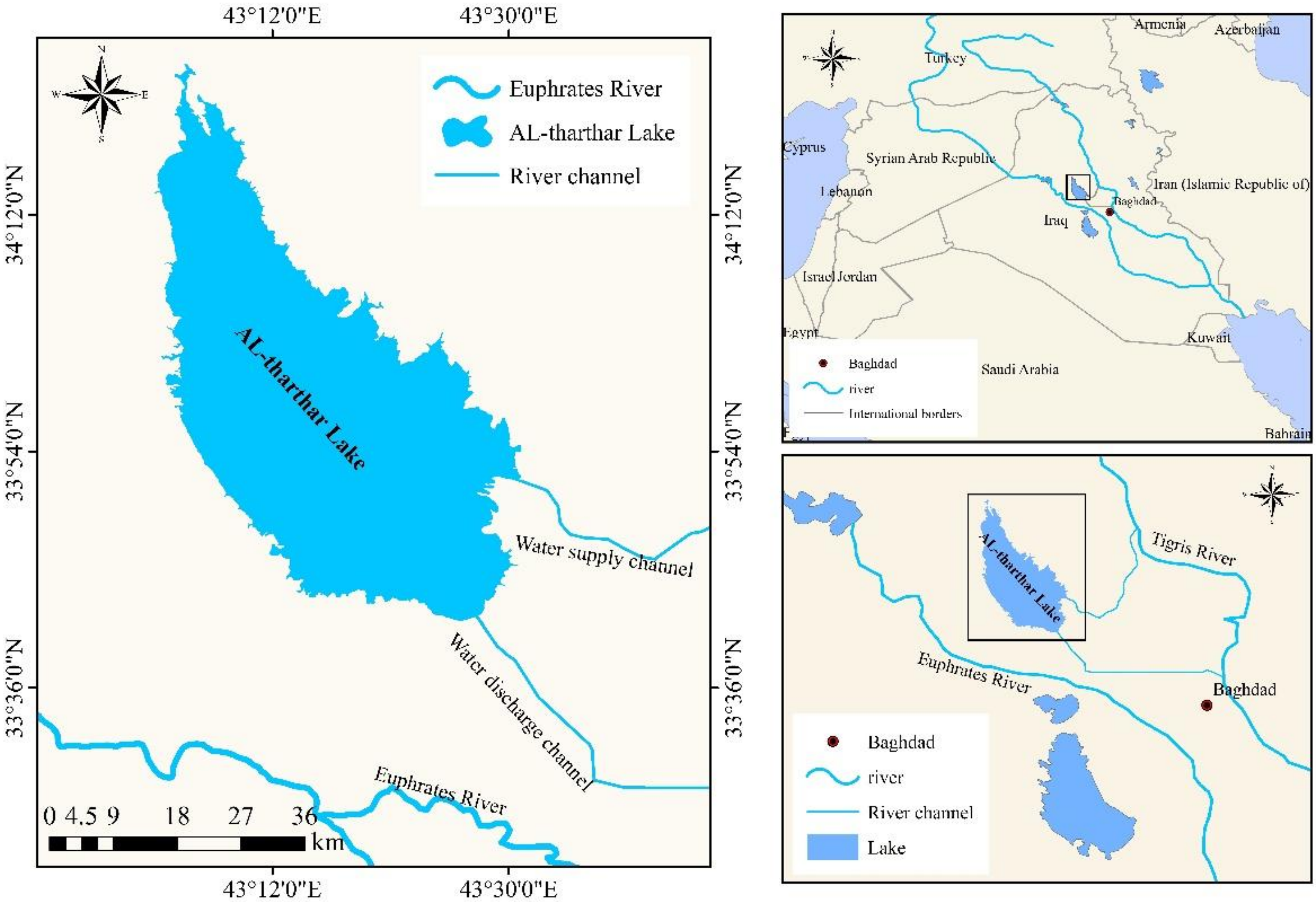


**Figure 2.** Geographical Location of Lake Tharthar and its Feeding and Drainage Channels.

## 2.2. Data Description

This study analyzes the spatial and temporal variations in LST and evaporation at Lake Tharthar by integrating thermal remote sensing data with meteorological data. To analyze the evaporation, the thermal remote sensing data of LST at Lake Tharthar was supplemented by meteorological data.

This study employs ground-based weather data collected from the Tikrit meteorological station (ID: 406340) from January to December 2023. This weather station encompasses major meteorological variables including air temperature (°C), relative humidity (%), wind speed and direction (m s⁻¹ and °), rainfall (mm), solar radiation (W m⁻²), and atmospheric pressure (hPa).

These data were obtained from the Iraqi Meteorological Organization and Seismology (IMOS), which operates a national network of ground-based weather stations. Quality control and homogenization procedures were applied to ensure data consistency and reliability prior to analysis.

Landsat 9 thermal infrared data were employed to augment ground-based meteorological observations and present spatially continuous information on the temperature of the lake surface. The long-term Landsat Earth observation record was extended by Landsat 9, which was launched in 2021. This mission boasts enhanced radiometric performance and stray light correction in comparison to its predecessors (Masek *et al.*, 2020; Lulla *et al.*, 2021). This study employed data from the Thermal Infrared Sensor-2 (TIRS-2) Band 10. This operates within the 10.6–11.2 µm spectral range and offers thermal measurements at a native resolution of 100 m, which is resampled to 30 m in standard products. (Cristóbal *et al.*, 2018;Bai & Wang, 2023). have extensively reported on the effectiveness of Band 10 in capturing thermal variability and retrieving water surface temperature across large inland water bodies.

All available Landsat 9 (OLI-2/TIRS-2) satellite imagery for 2023 spanning the Tharthar Lake Basin (path 169 and row 037) was accessed and processed using the GEE cloud computing platform. To obtain a cloud-free monthly representation, a total of 36 available satellite images were filtered throughout the year based on spatial boundaries, quality assessment ranges, and a cloud cover threshold of less than 10%. Using the GEE platform, these images were compiled monthly using the ImageCollection.median method, which resulted in 12 distinct monthly composite maps. Furthermore, the infrared thermal band 10, which has an original spatial resolution of 100 meters, was automatically resampled to 30 m within the GEE environment using multiple interpolations to match the spatial resolution of other optical bands when calculating surface temperature of the Earth, LST, and energy balance modeling.

**Table 1.** Metadata and spatial processing parameters for Landsat 9 images (path 169/row 037)

| Month | Landsat Series and Sensor | Acquisition Date (YYYY-MM-DD) | Path and Row | Band(s) Used | Native Spatial Resolution | Resampled Spatial Resolution |
|---|---|---|---|---|---|---|
| Jan | Landsat 9 OLI-2 / TIRS-2 | 2023-01-26 | 169 / 037 | Band 10 | 100 m | 30 m |
| Feb | Landsat 9 OLI-2 / TIRS-2 | 2023-02-27 | 169 / 037 | Band 10 | 100 m | 30 m |
| Mar | Landsat 9 OLI-2 / TIRS-2 | 2023-03-23 | 169 / 037 | Band 10 | 100 m | 30 m |
| Apr | Landsat 9 OLI-2 / TIRS-2 | 2023-04-16 | 169 / 037 | Band 10 | 100 m | 30 m |
| May | Landsat 9 OLI-2 / TIRS-2 | 2023-05-26 | 169 / 037 | Band 10 | 100 m | 30 m |
| Jun | Landsat 9 OLI-2 / TIRS-2 | 2023-06-27 | 169 / 037 | Band 10 | 100 m | 30 m |
| Jul | Landsat 9 OLI-2 / TIRS-2 | 2023-07-29 | 169 / 037 | Band 10 | 100 m | 30 m |
| Aug | Landsat 9 OLI-2 / TIRS-2 | 2023-08-30 | 169 / 037 | Band 10 | 100 m | 30 m |
| Sep | Landsat 9 OLI-2 / TIRS-2 | 2023-09-23 | 169 / 037 | Band 10 | 100 m | 30 m |
| Oct | Landsat 9 OLI-2 / TIRS-2 | 2023-10-25 | 169 / 037 | Band 10 | 100 m | 30 m |
| Nov | Landsat 9 OLI-2 / TIRS-2 | 2023-11-18 | 169 / 037 | Band 10 | 100 m | 30 m |
| Dec | Landsat 9 OLI-2 / TIRS-2 | 2023-12-20 | 169 / 037 | Band 10 | 100 m | 30 m |

## 2.3. Research Framework

### 2.3.1. Calculation of Lake Surface Temperature

Radiometric and thermal conversions were employed determine LST using satellite images. The thermal data captured by Landsat 9 Band 10 were subjected through a three-step process to estimate LST. The first step included conversion to radiance, followed by brightness temperature, and concluding with a correction to land surface temperature. This correction involved the surface emissivity (E), spectral thermal radiation (λ), constants like Planck's constant (h) and Boltzmann's constant (b), and celerity (c). This adjustment allowed us to reliably estimate the surface temperature rather than rely directly on the sensor-recorded data.

This process begins with the conversion of digital numbers (DN) from Landsat 9 thermal bands into spectral radiance through an inverse linear calibration function following Equation 1.

$$Radiance = \frac{L_{max} - L_{min}}{Qcal_{max} - Qcal_{min}} \times (DN - Qcal_{min}) \quad (1)$$

where $L_{max}$ is the maximum radiation value, $L_{min}$ is the minimum radiation value, $Qcal_{max}$ is the highest value taken by a pixel, $Qcal_{min}$ is the lowest value that (pixel) takes, and DN is the pixel value. Importantly, this equation integrates the maximum and minimum radiance values ($L_{max}$, $L_{min}$) with the associated quantized pixel values ($Qcal_{max}$, $Qcal_{min}$) to convert raw pixel data into physically meaningful radiance values (Oroud, 2020).

During the second stage, spectral radiance is transformed into at-sensor brightness temperature utilizing the Planck function (Eq. 4). The outcome of this stage indicates the effective temperature of the thermal band as measured by the sensor (Oroud, 2022) and is presented in Equation 2.

$$T = \frac{K_2}{ln\left(\frac{K_1}{Radiance} + 1\right)} \tag{2}$$

where $K_1$ and $K_2$ are 666.0932 and 1282.7201, respectively, for Landsat 9 OLI–TIRS (Oroud, 2022).

The concluding phase converts brightness temperature to surface temperature (ST), measured in degrees Celsius, following Equation 3.

$$\mathrm{ST} = \frac{\mathrm{BT}}{\left(1 + \lambda \times \frac{\mathrm{BT}}{\mathrm{C2}}\right)\ln(\mathrm{E})} \tag{3}$$

where BT refers to the highest atmospheric brightness temperature; λ represents the wavelength of the radiation emitted, which is 10 and 11 for Landsat 9 bands 10 and 11, respectively; and E is the emissivity of the Earth's surface as given in Equation 4.

$$C2 = h * c/s \tag{4}$$

where h is Planck's constant ($6.626 \times 10^{-34}$ J·s), kB (or s) is the Boltzmann constant ($1.38 \times 10^{-23}$ J/K), and c is the light velocity ($2.998 \times 10^{8}$ m/s).

### 2.3.2. METRIC Model Description

This study employed the METRIC (Mapping Evapotranspiration at High Resolution with Internalized Calibration) model to estimate evaporation from Lake Tharthar by resolving the surface energy balance using satellite-derived thermal data and ground-based meteorological observations. METRIC has been extensively applied in arid and semi-arid environments and is suitable for capturing spatially distributed evaporation under conditions of strong atmospheric forcing (Allen *et al.*, 2007). The model estimates latent heat flux (LE), which is directly related to evaporation, as the residual of the surface energy balance as presented in Equation 5.

$$\mathrm{LE} = \mathrm{R_n} - \mathrm{G} - \mathrm{H} \tag{5}$$

where latent heat flux (LE), related to evaporation, is determined by the net radiation ($R_n$) minus soil heat flux (G) and the sensible heat flux (H).

Landsat 9 TIRS-2 Band 10 thermal infrared data was used to derive LST, which is an important input to the calculation of sensible heat flux. The additional spectral bands were employed to derive surface albedo and emissivity, while simultaneous ground-based meteorological data from the Tikrit station air temperature and relative humidity, winds, and solar radiation provided the meteorological data required for the energy balance and stability corrections. Notably, METRIC is distinguished by its calibration method, which restricts the estimate of the reasonable range of sensible heat flux using two anchor pixels in the satellite image: "cold" pixel (maximum evaporation) and a "hot" pixel (minimum evaporation) (Allen *et al.*, 2007).

The calculation of sensible heat flux (H) is presented in Equation 6.

$$H = pacp\frac{\Delta T}{rah} \tag{6}$$

where air density is represented by rho_a, specific heat of air is c_p, ΔT is the temperature difference, and r_{ah} is aerodynamic resistance.

Subsequently, the equivalent evaporation rate (E) is calculated according to Equation 7.

$$= 3600\frac{Rn - G - H}{\lambda Pw} \tag{7}$$

where R_n represents the net radiation, G is the soil/water heat flux, λ is the latent heat of vaporization, rho_w is water density, and H is the sensible heat flux calculated from Equation 6.

METRIC yields instantaneous evaporation estimates at the time of satellite overpass. Subsequently, these estimates are converted to daily and seasonal evaporation totals using reference evapotranspiration ($ET_0$) derived from ground-based meteorological observations through the evapotranspiration fraction (ETrF) approach (Allen *et al.*, 2007). This hybrid framework integrates spatially distributed satellite information with point-based atmospheric data, thereby making METRIC particularly effective for estimating lake evaporation in arid regions characterized by strong spatial and temporal variability.

### 2.3.3. METRIC Model Validation and Accuracy Assessment

In order to guarantee the methodological reliability, reproducibility, and robustness of METRIC-derived evaporation estimates, an independent accuracy assessment framework was developed using machine learning techniques and implemented prior to the interpretation of spatiotemporal results. The validation strategy included a structured calibration–verification approach, which involved dividing the available dataset into training (80%) and testing (20%) subsets. This approach is widespread to reduce overfitting and facilitate an unbiased assessment of prediction performance (Das, 2025).

Model performance was evaluated using additional statistical measures such as Mean Squared Error (MSE) and Root Mean Squared Error (RMSE) (Zerouali *et al*., 2025). RMSE conveys the error in the original physical dimensions of evaporation, whereas the Nash Sutcliffe Efficiency (NSE) dimensionless scores the predictive competency of the models relative to the observed variability. Collectively, these metrics enable the comparison of model performance in different seasons and the assessment of absolute error.

Four machine learning algorithms were selected to encompass a broad range of modeling paradigms: Evolutionary Ensemble Deep Neural Network (EEDNN), Random Forest (RF), Spectral Angle Mapper (SAM), and Light Gradient Boosting Machine (LGBM).

These algorithms include deep learning, ensemble tree-based learning, spectral similarity analysis, and gradient boosting approaches, respectively, in order to facilitate a comprehensive assessment of METRIC-derived evaporation estimates under a variety of atmospheric and hydrological conditions. While capturing the nonlinear relationships and data-driven variability inherent in evaporation processes, using multiple algorithms improves the assessment of model stability and generalizability (Huang *et al*., 2022; Chen *et al*., 2025).

This study adopted the principle of neural networks, linked to machine learning principles, to test the accuracy of the METRIC model matrices (Das, 2025). This required a systematic framework to ensure that the results accurately reflect reality. The first verification step was calibration, where the model parameters were adjusted to minimize the discrepancy between simulated results and field observations (Zerouali *et al.*, 2025). This was followed by verification using independent data not used in the calibration phase. Accordingly, the data was divided into two parts.

- Training Data: Used to build the model.
- Testing Data: Used to evaluate the final performance of the model.

The data was divided into 80% for training purposes and 20% for verifying the results. In this context, statistical indicators should be used to quantify the deviation between the simulated and observed results. One such indicator was the efficiency of the Nash-Soutcliffe formula, which was used in water models to evaluate predictive ability, as expressed in the following mathematical formulas Equation 8.

- Mean Squared Error (MSE): Its importance lies its ability to give greater weight to large errors, thereby making it useful in improving the model to avoid highly inaccurate predictions (Goodarzi, *et al.*, 2025).

$$SE = \frac{1}{n}\sum_{i=1}^{n}(Q_{obs} - Q_{sim})^2 \qquad (8)$$

Where MSE is the mean squared error, n is the total number of observations, $Q_{obs}$ represents the observed evapotranspiration values, and $Q_{sim}$ represents the simulated values.

• Root Mean Square Error (RMSE):

This is the square root of the MSE. Notably, it restores the error to the original units of measurement and is the most commonly used indicator, as presented in Equation 9.

$$RMSE = \sqrt{\frac{1}{n}\sum_{i=1}^{n}(Q_{obs,i-} Q_{sim,i})^2} \qquad (9)$$

The root mean squared error (RMSE) measures the absolute value of the error in predicting the original units of a variable, thus, reflecting the degree of deviation between observed and simulated data.

For statistical acceptance criteria, calculating the relevant metrics alone is insufficient; it is also necessary to determine whether the resulting values indicate acceptable model performance (Zhang *et al.*, 2025). In hydrological studies, the following values are considered indicators of model quality:

• Nash-Sutcliffe Efficiency (NSE):

> 0.75: Excellent performance.

0.65–0.75: Very good performance.

0.50–0.65: Acceptable performance.

< 0.50: Poor performance (model is inaccurate).

## 3. Results and Discussion

### 3.1. Meteorological conditions

Meteorological conditions at Lake Tharthar during 2023 exhibited pronounced seasonal variability characteristic of the arid climate of western Iraq. Air temperature demonstrated a clear annual cycle, with minimum values recorded in winter and extreme heating occurring during summer. The lowest minimum temperature was recorded in January (3.2 °C), while maximum temperatures increased progressively through spring and reached a peak of 47 °C in July. Mean air temperatures exceeded 30 °C from May to September, which indicated sustained thermal stress during the warm season. Subsequently, a gradual cooling trend began in October, with mean temperatures decreasing to approximately 16 °C by December (Figure 3).

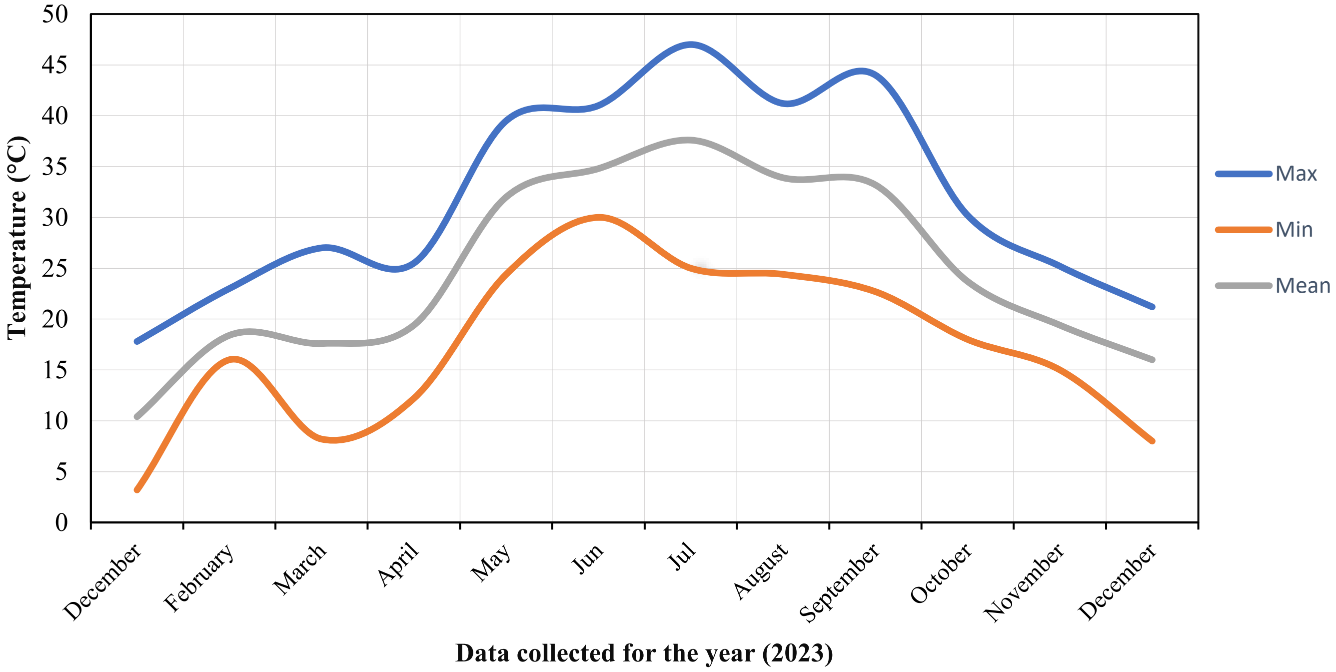


**Figure 3.** Monthly Changes in Air Temperatures (Maximum, Minimum, and Average) in Degrees Celsius Recorded at the Tikrit Climate Station During 2023.

Relative humidity and temperature displayed an inverse relationship. In the winter, humidity was higher, peaking at an 84% humidity level in February, which resulted in an evaporative demand. Meanwhile, the reverse was true in the summer, with July having the driest air of 19% humidity. This pattern of low humidity continued into August and September, following which it reversed in the fall and early winter. This relationship demonstrates how air temperature and humidity influence the evaporative demand on the surface air over a body of water (Figure 4).

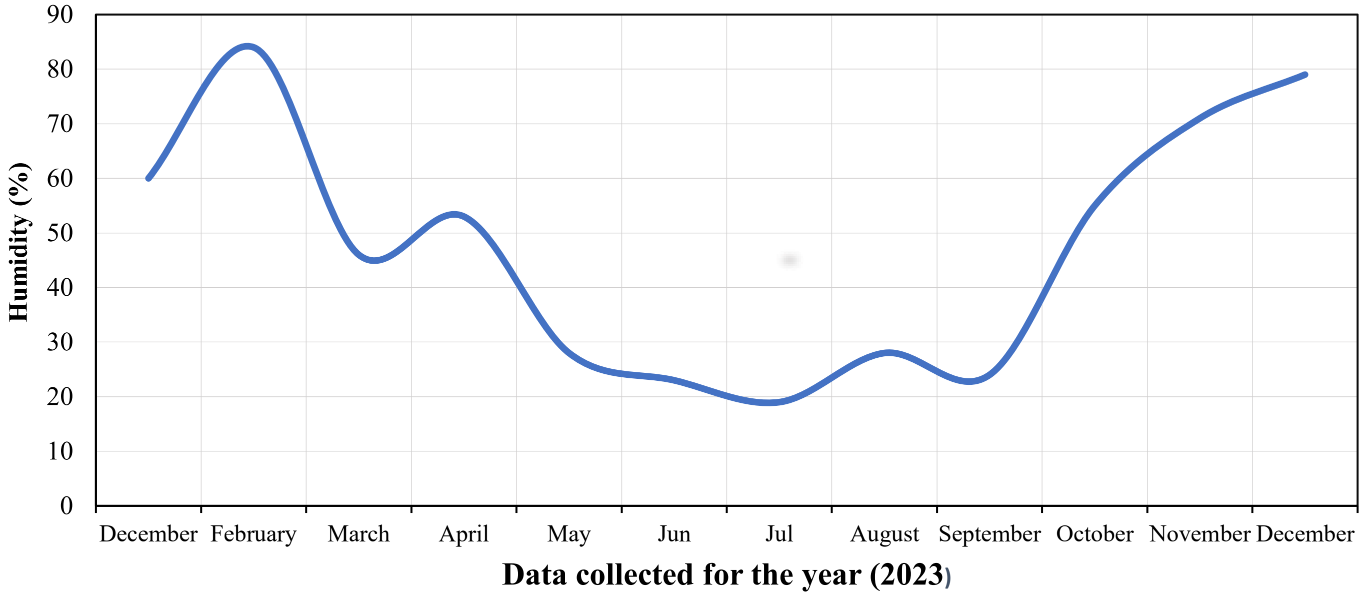


**Figure 4.** Monthly Average Relative Humidity (%) Recorded at the Tikrit Climate Station During 2023.

Seasonal changes were observed for wind speed, with the most notable changes occurring from winter to late spring. Wind speeds peaked in May at 31.7 m /s, but were stable during the summer, with average speeds from 9 to 10 m /s. Summer winds created favorable conditions to enhance evaporation increases. Wind speeds noticeably declined during November and December. These conditions created the appropriate seasonal framework for the surface heating and evaporation at the lake (Figure 5).

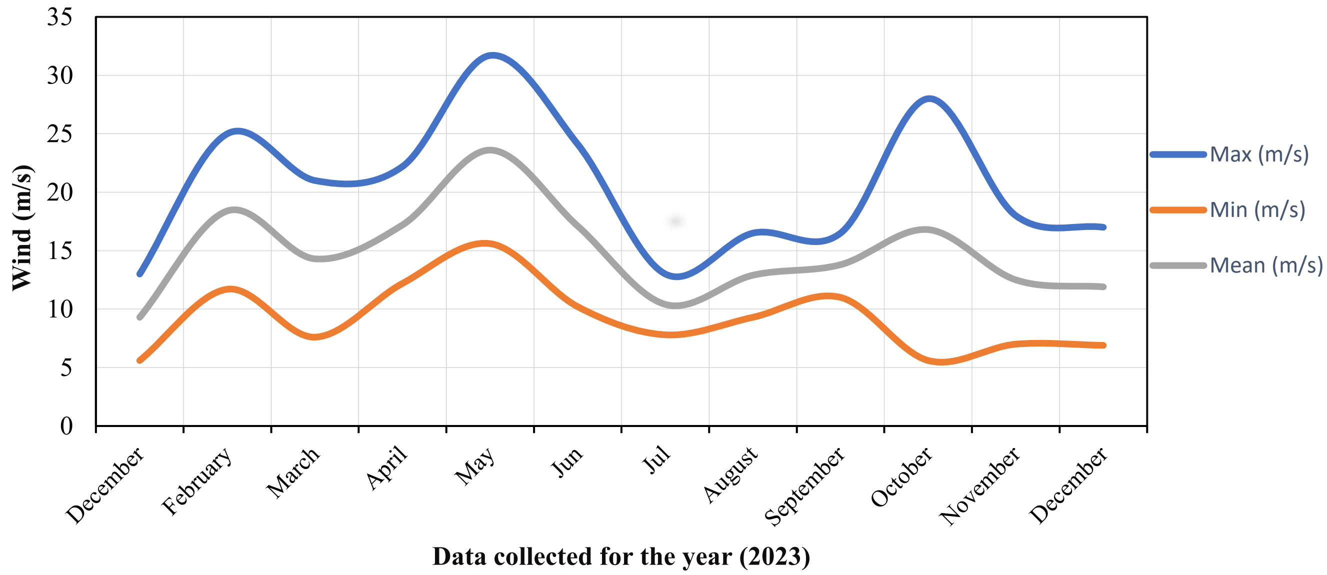


**Figure 5.** Monthly changes in wind speed (maximum, minimum, and average) in m/s recorded at the Tikrit climate station during 2023.

## 3.2. Lake Surface Temperature Variability

LST was measured using Landsat 9 and demonstrated seasonal and spatial variation across Lake Tharthar. Surface temperatures during January and February were below 15 °C, which was attributed to limited solar radiation and low atmospheric temperatures. Spring (March - May) marked the beginning of a warming trend, and surface temperatures were typically between 20 °C and 30 °C.

Lake surface temperatures were the highest in the summer months (June–August) with temperatures reaching 35 °C. In shallow and nearshore areas, surface temperatures exceeded 40 °C. During peak summer conditions, surface temperatures were high and peak air temperatures led to minimal relative humidity, thereby presenting ideal conditions for evaporation. During fall (September–November), surface air temperatures ranged from 20 °C to 30 °C. By December, the lake largely displayed surface temperatures below 20 °C, which signified the onset of cool seasonal conditions (Figure 6).

Nonetheless, LST was not constant across the entire lake. The shallow margins and southern section of the lake always displayed higher temperatures compared to the deeper central regions. This is because varying depths influence the storage of heat and exposure of the waters to the atmosphere, which consequently affected evaporation across the lake.

### 3.3. Spatial and temporal evaporation patterns

According to the METRIC based evaporation rates, evaporation patterns followed the seasonal patterns of changing surface lake temperatures and changing weather patterns. The lowest rates were observed during winter (January–February) when the average evaporation rate was less than 1 mm $h^{-1}$. This was primarily attributed to low temperatures, high relative humidity, and low thermal energy.

In spring (March–May), the first significant change in evaporation demand occurred. This season was characterized by the first substantial increases in evaporation rates, which averaged between 2 and 3 mm $h^{-1}$ and were driven by increasing temperatures and decreasing relative humidity. In the summer (June–August), evaporation demand peaked with several rates exceeding 4 mm $h^{-1}$. Notably, rates exceeded 5 mm $h^{-1}$ in the shallower, more exposed areas of the lake. Furthermore, the summer months also exhibited low relative humidity and high wind conditions, which increased the energy available for evaporation.

The cooling fall months (September–November) were characterized a decline in evaporation rates to 2–3 mm $h^{-1}$ due to decreasing temperatures and increased humidity. As in the previous winter, evaporation rates fell below 1 mm $h^{-1}$ by December. Spatial analysis revealed that evaporation rates were higher in the southern portions of the lake, which were shallower and more exposed to wind and less thermally inert, than in the center.

### 3.4. Model validation results

Algorithms are employed to illustrate the accuracy of the artificial neural network model in estimating evaporation. Neural networks, which estimate evaporation, rely on nonlinear climate data (temperature, humidity, wind data). To improve predictive accuracy, the model is trained using "training algorithms" that iteratively adjust weights and biases to minimize the cost function.

The hybrid integration of deep learning architectures and evolutionary algorithms to form Evolutionary Deep Neural Networks (EDNNS) represents a significant paradigm shift in hydrological and environmental modeling. Traditional backpropagation algorithms often struggle to process complex, nonlinear hydroclimatic data, and can become trapped in local minima, which potentially leads to overfitting during model optimization. EDNNS combines the multi-layered feature extraction capabilities with the exploratory search mechanisms of evolutionary algorithms (such as genetic algorithms (GA) or Particle Swarm Optimization (PSO) to systematically overcome the limitations of stepwise regression. This computational synergy allows dynamic structural optimization, flexible hyperparameter adjustment, and spatiotemporal concordance that surpasses traditional models, which ultimately leads to enhanced prediction accuracy and reduced uncertainty in surface evaporation estimates.

EDNNs rely on integrating two distinct methodologies to solve complex prediction problems: (1) the deep learning aspect, which consists of multiple layers of artificial neurons that allow the model to extract complex, nonlinear patterns from raw data (such as the interconnected relationships between temperature, rainfall, and stream flow); and (2) the evolutionary computation aspect, which comprises GA or PSO. Rather than following traditional methods like gradient descent, these algorithms are referred to as 'optimizers’ (Huang *et al*., 2022).

Spectral Angle Mapper (SAM): SAM is a popular algorithm for classifying satellite imagery, particularly in water quality studies using remote sensing. It measures the "spectral angle" between the spectral signature of each pixel in the image and a reference spectral signature of a specific water type (e.g., polluted water, muddy water, or chlorophyll-rich water) (Chen *et al.*, 2025). Importantly, SAM is able to map water quality over vast areas that cannot be covered by manual sampling, and integrates with models such as METRIC to provide accurate spatial data.

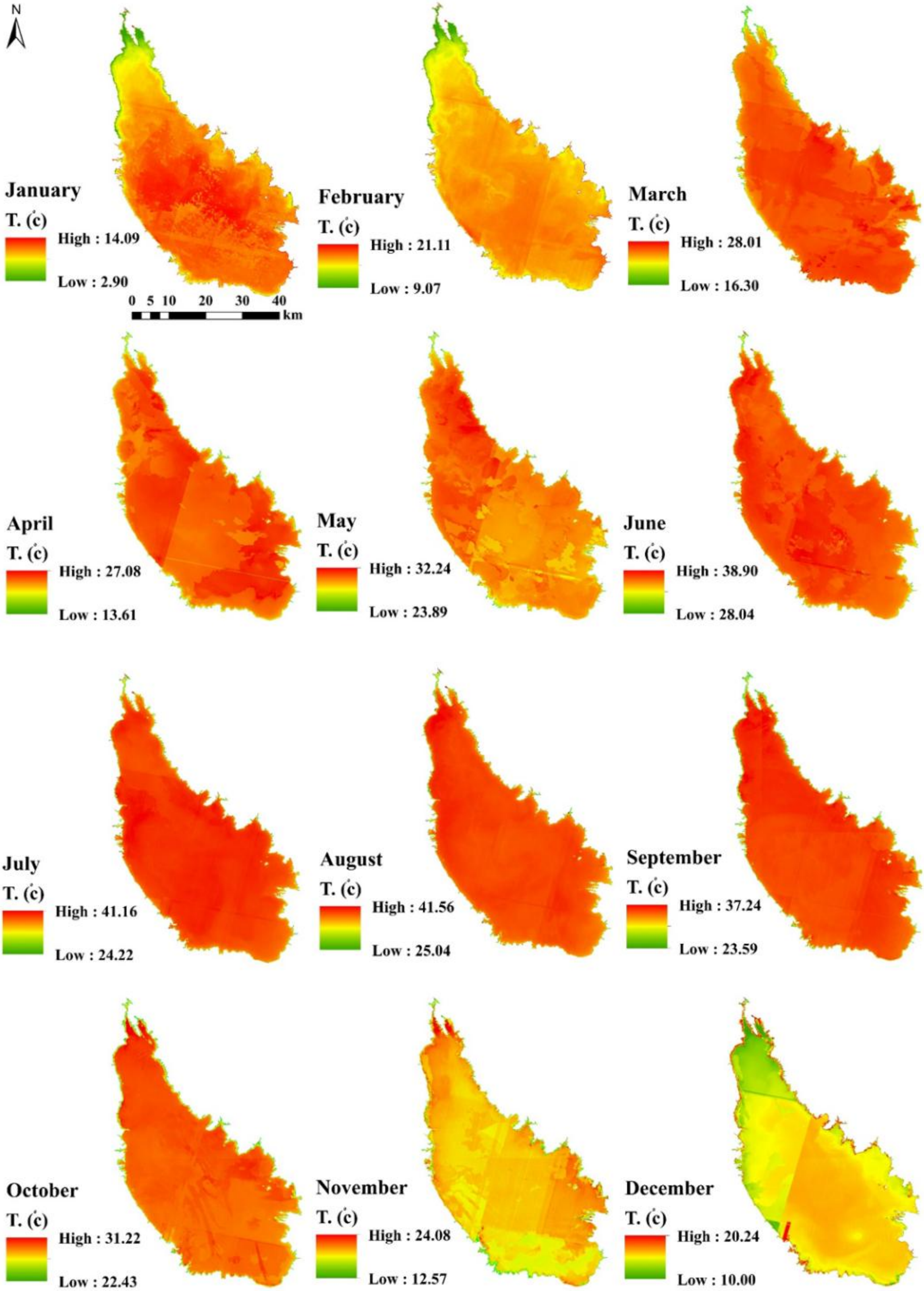


**Figure 6.** Spatial and Temporal Assessment of Free Thermal Pattern of the Surface of Lake Tharthar (°C) Derived from Satellite Imagery from 2023, Illustrating the Influence of Water Depth and Heat Capacity on the Heat Gain and Loss Distribution Across Seasons.

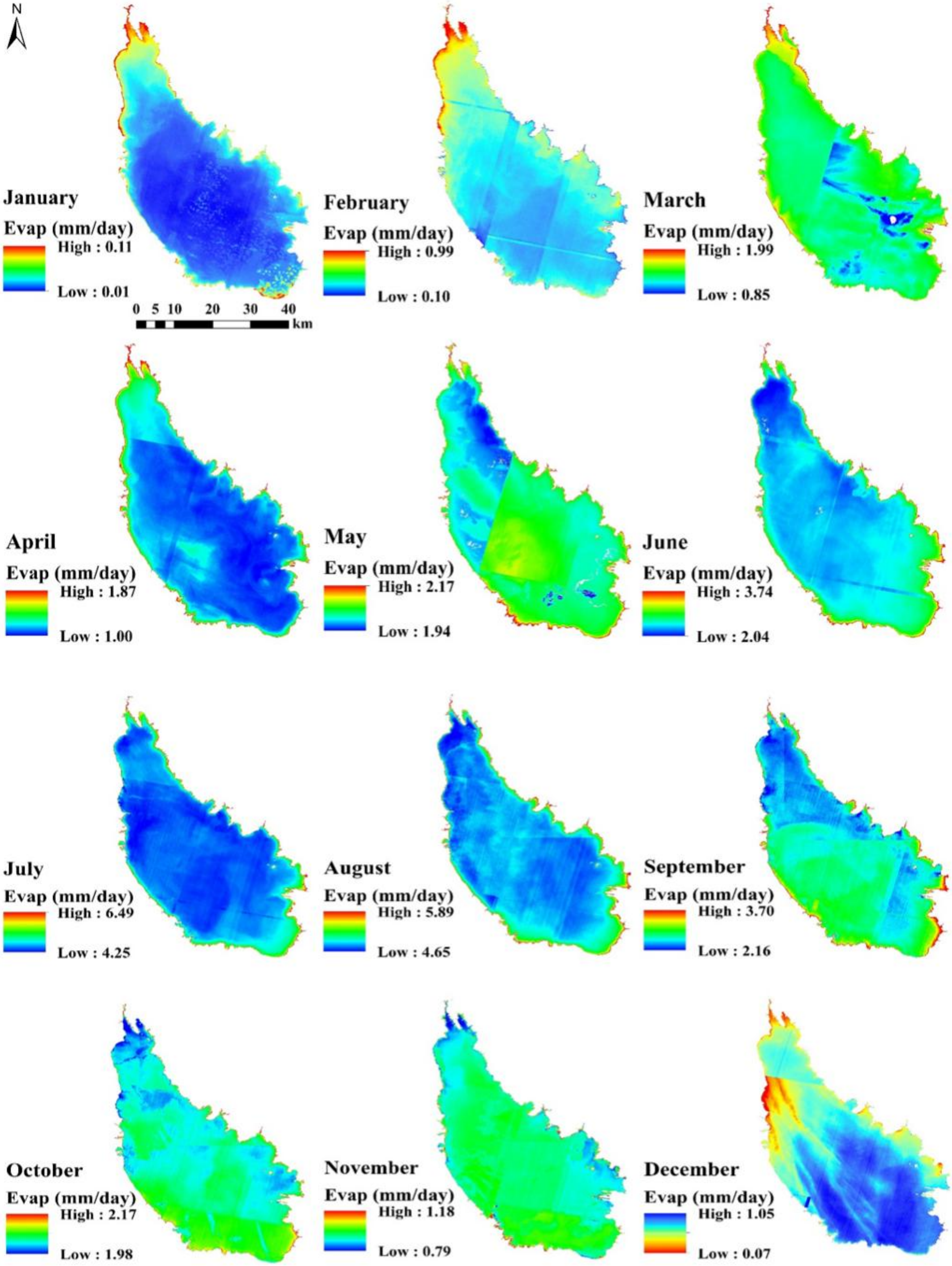


**Figure 7.** Spatial and Temporal Assessment of Daily Evaporation Rates (mm/day) of the Surface of Lake Tharthar Derived from Satellite Imagery from 2023, with Tracking of Seasonal Patterns and Impact of Climate Thermal Pattern Fluctuations on the Lake.

RF is one of the most efficient clustering models for modeling environmental and water relationships. It uses iterative clustering to build a wide network of independent decision trees during the training phase. The analytical depth of this algorithm lies in its ability to combine the outputs of individual trees through group voting or arithmetic mean, thereby effectively reducing computational variance and minimizing overmatch. Additionally, it offers high flexibility in assessing the relative importance of variables and handling complex nonlinear interactions and interrelationships between variable climatic elements (such as temperature, wind, and solar radiation) to produce highly stable and noise-tolerant predictions.

LGBM is an advanced, open-source gradient enhancement framework developed by Microsoft. Its computational architecture employs histogram-based algorithms and leaf-wise tree growth rather than balanced growth. In hydrological studies (Habibi & Tasouji Hassanpour, S., 2025), LGBM has emerged as a leading alternative to and competitor of the RF algorithm due to its exceptional ability to process time-series and high-dimensional spatial data with extremely high processing speed and relatively minimal memory consumption. Its relevance lies in its capacity to accurately model nonlinear energy and matter fluxes and surface-atmosphere interactions under extreme climatic conditions. In this context, LGBM is specifically used for:

• Flood prediction (due to its ability to handle real-time data at high speed)

• Estimating evaporation and transpiration (where the relationships between temperature, humidity, and wind are very complex)

• Predicting nitrate or phosphate concentrations (in long-term water quality models)

The statistical evaluation results of the Reference Remote Sensing (GEE) model display a high degree of hydrological agreement with the observed evaporation measurements from the Tikrit meteorological station (Table 2) and the simulated lake surface values. The total annual observed evaporation was 2,944 mm, compared to 2,813 mm for the simulated values, thereby reflecting the ability of the model to capture the overall dynamics of the hydrological cycle in the region with an annual cumulative difference of no more than 131.52 mm.

**Table 2.** Statistical Analysis and Error Differences Between Evaporation Measured at a Ground-based Meteorological Station and Evaporation Simulated Using Remote Sensing Data.

| **Month** | **Observed Evaporation $Q_{obs}$ (Tikrit - mm)** | **Simulated Evaporation $Q_{sim}$ (GEE - mm)** | **Difference Residual ($Q_{obs}$−$Q_{sim}$)** | **Monthly Squared Error ($Q_{obs}$−$Q_{sim}$)2** |
|---|---|---|---|---|
| January | 59.80 | 51.66 | 8.14 | 66.26 |
| February | 84.30 | 76.69 | 7.61 | 57.91 |
| March | 153.60 | 139.90 | 13.70 | 187.69 |
| April | 223.00 | 214.87 | 8.13 | 66.10 |
| May | 341.10 | 340.03 | 1.07 | 1.14 |
| June | 442.70 | 443.00 | -0.30 | 0.09 |
| July | 481.00 | 468.73 | 12.27 | 150.55 |
| August | 442.80 | 435.80 | 7.00 | 49.00 |
| September | 331.30 | 287.33 | 43.97 | 1,933.36 |
| October | 212.70 | 198.82 | 13.88 | 192.65 |
| November | 105.70 | 103.24 | 2.46 | 6.05 |
| December | 66.70 | 53.11 | 13.59 | 184.69 |
| Total Sum | 2,944.70 | 2,813.18 | 131.52 | 2,895.49 |

The efficiency of the modeling algorithms was particularly evident during the peak heat months (May, June, and July). Notably, the squared errors were lowest in June at 0.09 mm, a difference of only 0.30 mm, followed by May. This high accuracy indicates the excellent ability of the model to capture the interconnected nonlinear relationships among high temperatures, solar radiation, and wind speed during the summer.

Conversely, the model exhibited a marked variance in the forecast during September, and recorded as an absolute deviation of 43.97 mm between observed and simulated evaporation rates. This variance is primarily attributed to the complex thermal dynamics during the transition from late summer to autumn, when rapid changes in ambient air temperature coincide with a significant thermal inertia within the water mass of the lake. The resulting slowdown in thermal release from the deep-water reservoir alters the surface energy flux distribution, thereby complicating satellite-based thermal estimates and highlighting the need for higher-resolution space-based climate data.

Notably, the September error is the largest contributor to the overall assessment, accounting for over 66.7% of the total annual cumulative error squared. These results support the applicability of the model in hydrological planning, while underscoring the readjustment and calibration of algorithms during seasonal transition months to improve forecasting efficiency. These discrepancies arise from the nature of the transitional months: May marks the transition between spring and summer, while November characterizes the transition between autumn and winter. These periods are associated with rapid changes in solar radiation, angle of incidence, and air masses. Satellites calculate the thermal response of deep-water surfaces with a slowdown or acceleration that is distinct from the immediate response of field measurement basins. The effect of variations in the storage and surface area of the lake is also significant: May experiences the highest water levels in the Tharthar Lake due to water inflows and meltwater from the Tigris River, while the lowest water level are observed in November. This alters the hydrothermal capacity of the lake and influences remote sensing estimates compared to static measurements from the ground station.

Field comparison of the tested models revealed that EEDNN achieved the highest accuracy for evaporation prediction, with a minimum deviation of 4.96 mm. The RF model ranked second with high efficiency, and had a deviation of 5.21 mm. The LGBM model followed in third place (Table 3), while the SAM algorithm ranked fourth and demonstrated the lowest predictive accuracy among the evaluated machine learning models. In contrast, the direct remote sensing model (GEE Model) exhibited the highest uncertainty level at 15.53, thereby statistically demonstrating that relying solely on remote sensing techniques is insufficient, and that integrating these techniques with deep learning algorithms is essential for improving the accuracy of hydrological estimates.

**Table 3.** Evaluation and Ranking of Machine Learning and Remote Sensing (GEE) Models Based on Mean Squared Error (MSE) and Root Mean Squared Error (RMSE).

| **Model** | **Mean Squared Error (MSE)** | **Root Mean Squared Error (RMSE) mm/month** | **Evaluation & Overall Ranking** |
|---|---|---|---|
| EEDNN | 24.63 | 4.96 mm | 1st Place: Best & Highest Accuracy (Lowest Error Rate) |
| RF | 27.14 | 5.21 mm | 2nd Place: Excellent Performance & Very Close to Best |
| LGBM | 33.66 | 5.80 mm | 3rd Place: Moderate Quality |
| SAM | 41.42 | 6.44 mm | 4th Place: Lowest Accuracy Among ML Models |
| GEE Model | 241.29 | 15.53 mm | Baseline RS Model: High Regional Coverage (Higher Uncertainty) |

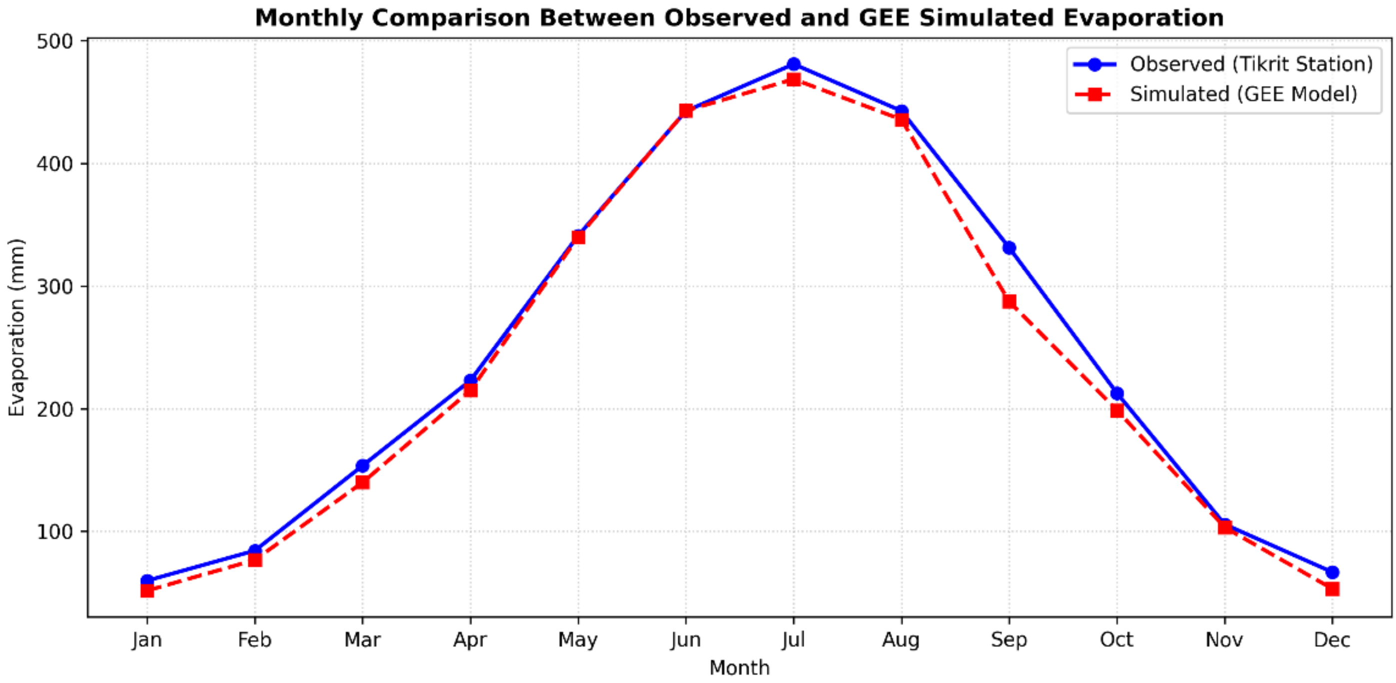


**Figure 8.** Monthly Change in Evaporation Rates Measured in the Field and Simulated via Remote Sensing Platform (GEE).

Figure 8 illustrates the consistency and adherence to the general seasonal pattern of evaporation between the values observed at the Tikrit station and the values simulated by remote sensing from the GEE platform, with a peak in July and a decline during the winter months. Further, The measurements align closely during the summer months (May, June, and August), reflecting the model's high accuracy in representing periods of high evaporation. Notably, the largest deviation between the actual and simulated curves is observed during September, where the model continues to exhibit a slight underestimation tendency for most of the year.

## 4. Discussion

The findings of this study demonstrate that atmospheric forcing is the primary control mechanism for lake evaporation in arid contexts. Lake Tharthar is a lucid example of the interaction between temperature, humidity, and wind, and their joint effect on energy transfer from the surface to the atmosphere. Seasonal patterns indicate that evaporation is impacted by climatic drivers in a non-linear, episodic manner. Evaporation is strongest when the conditions are extremely hot and dry, and is weakest when the conditions are cool and humid. This aligns with the established and well-supported theoretical and empirical frameworks of the evaporation processes in arid and semi-arid contexts, where the demand for atmospheric moisture is often greater than the supply (Siadatmousavi & Seyedalipour, 2019; Lobos-Roco *et al*., 2021).

Moreover, the results of this study reveal the non-uniform nature of evaporation across Lake Tharthar. Although each spatial pattern example is unique, they are all considerably affected by lake morphology, thermal inertia, and exposure to the atmosphere. There is a clear evaporation preference in the shallow, southern, and peripheral parts of the lake compared to the deeper, central parts of the lake. This is likely due to shorter evaporation rates, susceptibilities, and the heat retention capacity of the lake. Across various lakes, studies have been demonstrated that shallow water bodies (especially the peripheral regions of lakes) serve as evaporation hotspots. This is attributed to rapid evaporation from the lake surface due to differences in heating, synthesis of energy, and its interaction with the atmosphere (Shao *et al*., 2020; Holman *et al*., 2023). The findings of the present study are consistent with this pattern and further support previous observations that shallow lake margins can function as evaporative hotspots.

The impact of wind on evaporation is spatially differentiated and accentuated by wind fetch. In areas of high fetch, wind promotes turbulence, which increases the evaporation rate from the lake surface. It has been demonstrated that the evaporation rate from the lake may differ due to the varying exposure of the lake to wind, even under a relatively homogeneous climate in the region. Sugita *et al*. (2020) and Farooq *et al*. (2022) suggest that evaporation may be enhanced in a localized area due to differing vapor pressure, surface roughness, and uneven roughness of the lake surface. It is evident from these findings that the evaporation processes of the lake are best captured through modeling the surface of the lake. Simplified methods, which represent a unit of space as a single point or use coarse aggregate values, fundamentally misrepresent the evaporation from large lakes that exhibit a high degree of morphological and spatial variability.

These results validate METRIC for modeling lake evaporation in different environments, including arid, semi-arid, and agricultural regions (Danodia *et al*., 2024; Iqbal *et al*., 2024). Particularly, data-scarce countries benefit from the internal calibration method using hot and cold pixels as it does not depend on extensive meteorological networks, while also providing high accuracy (Allen *et al*., 2007; Acharya *et al*., 2020). Unlike other energy balance approaches, METRIC can provide reliable and accurate estimates for evaporation in agricultural and semi-arid areas with a patchy land cover (Khand *et al*., 2021; Mondal *et al*., 2022; Rahimi *et al*., 2021).

The integration of METRIC and machine learning–based validation within the methodological framework strengthens the design by allowing the uncertainty and performance to be expressed comprehensively across various modeling approaches. Moreover, this framework advances the interpretability of the modeling results and provides a valid framework for using satellite-based estimates of evaporation in the planning and management of water resources where in situ measurements are sparse or lacking.

Therefore, the framework described here for the estimation of evaporation from Lake Tharthar in Iraq is innovative and extremely useful. However, despite its strengths, the methodology also has a few limitations. The first and most notable limitation is the use of meteorological data from a single weather station. This is likely to overlook the microclimatic variability within the area of Lake Tharthar, and particularly within the considerable area of this region. The challenge remains to better represent the spatial atmospheric gradients by using reanalysis products or by extending ground-based observation networks.

Second, the 16-day revisit cycle for Landsat data is likely to mask the evaporative response from synoptic weather events. Moreover, the spatial and atmospheric resolution of the data may be improved further by using MODIS or Sentinel data. Data fusion methodologies have exhibited promising results in combining high spatial resolution with high temporal data.

Third, drawing representative hot and cold pixels adds some level of subjectivity that could impact model results, even though METRIC internal calibration lessens the need for field data collection. Thus, future studies should focus on hybrid calibration techniques to diminish uncertainties further. Additionally, the inclusion of eddy covariance or scintillometry data to enhance validation efforts would add more focused bounds to energy flux estimates. This multi-faceted approach will optimize lake evaporation estimation and enable the application of adaptive water management techniques to react to evolving climatic conditions.

To compare these results with their regional and broader context, the evaporation dynamics of Lake Tharthar were evaluated in comparison with previous studies conducted in water bodies with extremely arid and semi-arid environmental, and in geographical conditions in the Middle East and North Africa. The pronounced seasonal variation in LST, ranging from below 15 °C in winter to above 40 °C in shallow areas in summer, is consistent with findings reported for regional lakes such as Lake Urmia in Iran (Tasumi, 2019; Javadian *et al*., 2019) and the Dead Sea (Oroud, 2020), where high solar irradiance and severe vapor pressure deficits contribute to extreme evaporative responses (Farooq *et al*., 2025). In contrast to reservoirs in semi-arid Mediterranean climates, such as Lake Qaraoun in Lebanon (Mhawej *et al*., 2020) and Lake Oubira in Algeria (Rezzag Bara *et al*., 2019), where coastal humidity limits water loss (Zhao *et al*., 2022), Lake Tharthar experiences accelerated evaporation due to strong dry winds, reaching 31.7 m/s, and summer temperatures reaching up to 47 °C. The observed spatial pattern, in which shallow lake margins form evaporation hotspots relative to the deeper central basin, can be attributed to morphometric differences in water heat capacity and thermal inertia. These findings are consistent with the physical models proposed by Shao *et al*. (2020) and Zhang *et al*. (2024).

More broadly, the findings of this study are directly linked to several United Nations Sustainable Development Goals. The precise quantification of annual evaporation losses (exceeding 2.93 billion cubic meters) contributes to Goal 6: Clean Water and Sanitation (sub-goal 6.4) by providing accurate data to improve water use efficiency and manage water scarcity in the strategic reservoirs of Iraq. Furthermore, identifying the high climate sensitivity of the lake supports Goal 13: Climate Action (sub-goal 13.1) by offering a practical remote sensing tool to enhance adaptation and strengthen climate resilience against desertification and drought. Finally, identifying the shallow shorelines most vulnerable to rapid degradation provides a scientific baseline for wetland protection under Goal 15: Life on Land (sub-goal 15.3), thereby supporting efforts to combat land degradation and maintain ecosystems in arid environments.

## 5. Conclusion

This study applied the METRIC model using thermal data from the Landsat 9 satellite and combined it with terrestrial meteorological observations to estimate evaporation rates and assess heat exchange between the lake and atmosphere across seasons. By leveraging advanced satellite thermal remote sensing techniques, this study provides a robust framework for measuring heat fluxes in data-poor arid environments, such as Iraq.

These results emphasize the important role of evaporation in water loss from Lake Tharthar and its implications for water resource management in Iraq. Accurately quantifying evaporation is necessary to ensure the operation of reservoirs, plan flood control, and allocate water over the long term under increasing climatic stress. This technique generates spatially distinct information that can be used to support targeted management strategies, such as prioritizing monitoring efforts in high-loss zones and assessing the feasibility of evaporation-reduction measures.

To better represent spatial atmospheric gradients, future research should aim to integrate higher-temporal-resolution satellite data in order to capture short-term variability in evaporation, expand ground-based meteorological networks, and explore data-fusion approaches that combine physical models with advanced machine learning techniques. These advancements will enhance adaptive water management strategies and facilitate accurate evaporation monitoring in arid and semi-arid regions experiencing growing water scarcity.

**Acknowledgements**

The researchers express their gratitude to the University of Anbar and Higher Institute of Desert Sciences for their support for studies concerning climate change and its effects on water resources in Iraq.

**Author Contributions**

**Conceptualization**: Author Salh, A. M., Ali, B. B.; **methodology**: Salh, A. M., El Kenawy; **investigation**: Salh, A. M., Chiad, S. I , Muslih, K. d.; **writing—original draft preparation**: Salh, A. M., El Kenawy, Chiad, S. I ; **writing—review and editing**: Kenawy, Chiad, S. I. Ali, B. B; **visualization**:. All authors have read and agreed to the published version of the manuscript.

**Conflict of interest**

All authors declare that they have no conflicts of interest.

**Data availability**

Data is available upon request.

**Funding**

This research received no external funding.

## References

Abdullah, M., Al-Ansari, N., & Laue, J. (2019). Water resources projects in Iraq: reservoirs in the natural depressions. *Journal of Earth Sciences and Geotechnical Engineering*, 9(4), 137-152.

Abir, S., H. A. McGowan, Y. Shaked, H. Gildor, E. Morin & N. G. Lensky (2024). Air–sea interactions in stable atmospheric conditions: lessons from the desert semi-enclosed Gulf of Eilat (Aqaba). *Atmospheric Chemistry and Physics* 24(10): 6177-6195. doi.org/10.5194/acp-24-6177-2024

Acharya, B., V. Sharma, J. Heitholt, D. Tekiela and F. Nippgen (2020). Quantification and Mapping of Satellite Driven Surface Energy Balance Fluxes in Semi-Arid to Arid Inter-Mountain Region." *Remote Sensing* 12(24): 4019. doi.org/10.3390/rs12244019

Ahmood, B. B., Hamza, Z. A., & Al-Hadithi, M. (2024). An Overview of the Remote Sensing and GIS Techniques Application to Detect Changes in the Surface Area of Water Bodies in Iraq. *The Iraqi Geological Journal*, 263-274. doi.org/10.46717/igj.57.1D.20ms-2024-4-30

Al-Daghistani, N. S., (2003). Remote Sensing Basics and Applications. (first edition). Dar Al-Manhaj for Publishing and Distribution, Al-Balagha Applied University, p.243.

Ali, A., Y. Al-Mulla, Y. Charabi, G. Al-Rawasm & M. Al-Wardy (2021). Remote Sensing Approach for Estimating Evapotranspiration Using Satellite-Based Energy Balance Models in Al Hamra, Oman. *Advances in Science, Technology & Innovation*, Springer International Publishing: 73-79.

Allen, R. G., M. Tasumi and R. Trezza (2007). Satellite-Based Energy Balance for Mapping Evapotranspiration with Internalized Calibration (METRIC)—Model. *Journal of Irrigation and Drainage Engineering* 133(4): 380-394. doi.org/10.1061/(ASCE)0733-9437(2007)133:4(380)

Allen, R. G., Tasumi, M., Morse, A., & Trezza, R. (2005). Satellite-based evapotranspiration by energy balance for western states water management. In *Impacts of Global Climate Change* (pp. 1-18). doi.org/10.1061/40792(173)556

Allen, R. G., Trezza, R., Kilic, A., Tasumi, M., & Li, H. (2013). Sensitivity of Landsat-scale energy balance to aerodynamic variability in mountains and complex terrain. *JAWRA Journal of the American Water Resources Association*, 49(3), 592-604. doi.org/10.1111/jawr.12055

Al-Obaidi, Gh. Y. A., (2009). Determining the flood area of the water body and land uses of Tharthar Lake, west of Baghdad, using satellite data from the Aqua MODIS satellite, *Al-Rafidain Engineering*, Volume 17, Issue 6.

Alsumaiei, A. A. (2025). Improving Evaporative Loss Forecasts in Arid Climates by Integrating Machine Learning Models With Feature Selection Algorithms. *JAWRA Journal of the American Water Resources Association* 61(3). doi.org/10.1111/1752-1688.70025

Bai, P. & Y. Wang (2023). The Importance of Heat Storage for Estimating Lake Evaporation on Different Time Scales: Insights From a Large Shallow Subtropical Lake. *Water Resources Research* 59(9). doi.org/10.1029/2023WR035123

Bastiaanssen, W. G., Menenti, M., Feddes, R. A., & Holtslag, A. A. M. (1998). A remote sensing surface energy balance algorithm for land (SEBAL). 1. Formulation. *Journal of Hydrology*, 212, 198-212. doi.org/10.1016/S0022-1694(98)00253-4

Biggs, T. W., Petropoulos, G. P., Velpuri, M. N., Marshall, M., Glenn, E. P., Nagler, P., & Messina, A., (2016). Remote sensing of actual evapotranspiration from croplands. In: Thenkabail, P.S. (Ed.), *Remote Sensing of Water Resources, Disasters, and Urban Studies*, Volume III of Remote Sensing Handbook. CRC Press, FL, p. 59–100.

Chávez, J. L., P. H. Gowda, T. A. Howell & K. S. Copeland (2009). Radiometric surface temperature calibration effects on satellite based evapotranspiration estimation. *International Journal of Remote Sensing* 30(9): 2337-2354. doi.org/10.1080/01431160802549393

Chen, H., Chu, N., Kang, A., Wang, W., & He, J. (2025). Simulation and analysis of evapotranspiration from desert grasslands based on a random forest regression model. *Scientific Reports*, 15(1), 25760. doi.org/10.1038/s41598-025-11056-0

Cristóbal, J., Jiménez-Muñoz, J. C., Prakash, A., Mattar, C., Skoković, D., & Sobrino, J. A. (2018). An improved single-channel method to retrieve land surface temperature from the Landsat-8 thermal band. *Remote Sensing*, 10(3), 431. doi.org/10.3390/rs10030431

Danodia, A., N. R. Patel, K. Suresh, R. P. Singh, A. Satpathi, P. Chauhan and N. A. S (2024). "Quantifying energy fluxes in Tarai region of India during post-monsoon season: Insights from METRIC model, ET station and remote sensing." *Journal of Agrometeorology* 26(3): 271-278. doi.org/10.54386/jam.v26i3.2618

Das, A. (2025). An optimization based framework for water quality assessment and pollution source apportionment employing GIS and machine learning techniques for smart surface water governance. *Discover Environment*, 3(1), 1-35. doi.org/10.1007/s44274-025-00327-2

Fadel, A., M. Mhawej, G. Faour and K. Slim (2020). On the application of METRIC-GEE to estimate spatial and temporal evaporation rates in a mediterranean lake. *Remote Sensing Applications: Society and Environment* 20: 100431. doi.org/10.1016/j.rsase.2020.100431

Fadel, B. A. and H. S. Najiban (2024). "Estimate of the Surface Evaporation from the Tharthar Lake (Buhayrat Tharthar) in Iraq, Based on Remote Sensing Data and Techniques of Geographic Information Systems GIS." *International Journal of Religion* 5(9): 370-379.

Farooq, U., H. Liu, Q. Zhang, Y. Ma, J. Wang and L. Shen (2022). Spatial variability of global lake evaporation regulated by vertical vapor pressure difference. *Environmental Research Letters* 17(5): 054006. doi.org/10.1088/1748-9326/ac614b

Farooq, U., Liu, H., Zhang, Q., Wang, J., & Shen, L. (2025). Global lake evaporation estimates by integrating penman method with equilibrium temperature approach. *Journal of Hydrometeorology*, 26(9), 1301-1313. doi.org/10.1175/JHM-D-24-0146.1

Forootan, E. (2019). Analysis of trends of hydrologic and climatic variables. *Soil and Water Research* 14(3): 163-171. doi.org/10.17221/154/2018-SWR

Goodarzi, A., Sergini, M. M., Saber, A., Shadkani, S., Pak, A., & Rezazadeh, F. (2025). Prediction of pan evaporation across diverse climates and scenarios using temporal attention clockwork recurrent neural networks coupled with long short-term memory. *Water Cycle*, 6, 241-253. doi.org/10.1016/j.watcyc.2025.03.002

Habibi, S., & Tasouji Hassanpour, S. (2025). An Explainable Machine Learning Framework for Forecasting Lake Water Equivalent Using Satellite Data: A 20-Year Analysis of the Urmia Lake Basin. *Water*, 17(10), 1431. doi.org/10.3390/w17101431

Holman, K. D., K. M. Mikkelson and D. K. Llewellyn (2023). "Characterizing Spatial Heterogeneity in Reservoir Evaporation within the Rio Grande Basin Using a Coupled Version of the Weather, Research, and Forecasting Model." *Journal of Hydrometeorology* 24(9): 1437-1456. doi.org/10.1175/JHM-D-22-0210.1

Huang, H., Wang, W., Lv, J., Liu, Q., Liu, X., Xie, S., ... & Feng, J. (2022). Relationship between chlorophyll a and environmental factors in lakes based on the random forest algorithm. *Water*, 14(19), 3128. doi.org/10.3390/w14193128

Hussain, R. Y. (2024). Bathymetric Map Production of Therthar Depression Basin and Water Storage Volume Estimation. *Diyala Journal of Engineering Sciences*, 32-44. doi.org/10.24237/djes.2024.17303

Iqbal, M. M., M. Abdullah and T. Rashid (2024). "Estimation of evapotranspiration using METRIC model with high resolution." *Big Data in Water Resources Engineering (BDWRE)* 5(2): 58-62. doi.org/10.26480/bdwre.02.2024.58.62

Javadian, M., A. Behrangi, M. Gholizadeh and M. Tajrishy (2019). "METRIC and WaPOR Estimates of Evapotranspiration over the Lake Urmia Basin: Comparative Analysis and Composite Assessment." *Water* 11(8): 1647. doi.org/10.3390/w11081647

Khand, K., Bhattarai, N., Taghvaeian, S., Wagle, P., Gowda, P. H., & Alderman, P. D. (2021). Modeling evapotranspiration of winter wheat using contextual and pixel-based surface energy balance models. *Transactions of the ASABE*, 64(2), 507-519. doi.org/10.13031/trans.14087

Laounia, N., H. Abderrahmane, K. Abdelkader, S. Zahira and Z. Mansour (2017). Evapotranspiration and Surface Energy Fluxes Estimation Using the Landsat-7 Enhanced Thematic Mapper Plus Image over a Semiarid Agrosystem in the North-West of Algeria. *Revista Brasileira de Meteorologia* 32(4): 691-702. doi.org/10.1590/0102-7786324016

Li, Z. L., Tang, R., Wan, Z., Bi, Y., Zhou, C., Tang, B., ... & Zhang, X. (2009). A review of current methodologies for regional evapotranspiration estimation from remotely sensed data. *sensors*, *9*(05), 3801-3853. doi.org/10.3390/s90503801

Lima, J. G., Sánchez, J. M., Piqueras, J. G., Espínola Sobrinho, J., Viana, P. C., & Alves, A. D. S. (2020). Evapotranspiração do sorgo a partir do balanço de energia por METRIC e STSEB. *Revista Brasileira de Engenharia Agrícola e Ambiental*, *24*, 24-30. doi.org/10.1590/1807-1929/agriambi.v24n1p24-30

Lobos-Roco, F., Hartogensis, O., Vilà-Guerau de Arellano, J., De La Fuente, A., Muñoz, R., Rutllant, J., & Suárez, F. (2021). Local evaporation controlled by regional atmospheric circulation in the Altiplano of the Atacama Desert. *Atmospheric Chemistry and Physics*, *21*(11), 9125-9150. doi.org/10.5194/acp-21-9125-2021

Lulla, K., M. D. Nellis, B. Rundquist, P. K. Srivastava and S. Szabo (2021). Mission to earth: LANDSAT 9 will continue to view the world. *Geocarto International* 36(20): 2261-2263. doi.org/10.1080/10106049.2021.1991634

Lyons, E. A., & Sheng, Y. (2017). LakeTime: Automated seasonal scene selection for global lake mapping using Landsat ETM+ and OLI. *Remote Sensing*, *10*(1), 54.doi.org/10.3390/rs10010054

Maleki, S., S. H. Mohajeri, M. Mehraein and A. & Sharafati (2024). Lake evaporation in arid zones: Leveraging Landsat 8's water temperature retrieval and key meteorological drivers. *Journal of Environmental Management* 355: 120450. doi.org/10.1016/j.jenvman.2024.120450

Masek, J. G., M. A. Wulder, B. Markham, J. McCorkel, C. J. Crawford, J. Storey and D. T. Jenstrom (2020). Landsat 9: Empowering open science and applications through continuity. *Remote Sensing of Environment* 248: 111968. doi.org/10.1016/j.rse.2020.111968

Matta, E., Amadori, M., Free, G., Giardino, C., & Bresciani, M. (2022). A satellite-based tool for mapping evaporation in inland water bodies: Formulation, application, and operational aspects. *Remote Sensing*, 14(11), 2636. doi.org/10.3390/rs14112636

Mhawej, M., A. Fadel and G. Faour (2020). Evaporation rates in a vital lake: a 34-year assessment for the Karaoun Lake. *International Journal of Remote Sensing* 41(14): 5321-5337. doi.org/10.1080/01431161.2020.1739354

Micijevic, E., Haque, M. O., Scaramuzza, P., Storey, J., Anderson, C., & Markham, B. (2019). Landsat 9 pre-launch sensor characterization and comparison with Landsat 8 results. In *Sensors, Systems, and Next-Generation Satellites XXIII* (Vol. 11151, pp. 289-300). SPIE. doi.org/10.1117/12.2533102

Mondal, I., S. Thakur, A. De and T. K. De (2022). Application of the METRIC model for mapping evapotranspiration over the Sundarban Biosphere Reserve, India. *Ecological Indicators* 136: 108553. doi.org/10.1016/j.ecolind.2022.108553

Oroud, I. M., (2019). The utility of thermal satellite images and land-based meteorology to estimate evaporation from large lakes. *Journal of Great Lakes Research*, 45(4), p. 703-714. doi.org/10.1016/j.jglr.2019.05.004

Oroud, I. M. (2020). Spatial and temporal surface temperature patterns across the Dead Sea as investigated from thermal images and thermodynamic concepts: IM Oroud. *Theoretical and Applied Climatology*, *142*(1), 569-579. doi.org/10.1007/s00704-020-03343-9

Oroud, I. M., (2022). Derivation of spatially distributed thermal comfort levels in Jordan as investigated from remote sensing, GIS tools, and computational methods. *Theoretical and Applied Climatology*, 148(1-2), 569-583. doi.org/10.1007/s00704-022-03951-7

Rahimi, A., Bouasria, A., Bounif, M., Zaakour, F., & El Mjiri, I. (2021). Estimating evapotranspiration using remote sensing and the METRIC energy balance model: case study of Sidi Benour region (Morocco). In *2021 Third International Sustainability and Resilience Conference: Climate Change* (pp. 142-147). IEEE. doi.org/10.1109/IEEECONF53624.2021.9667981

Rezzag Bara, C., Djidel, M., Medjani, F., & Labar, S. (2019). Spatiotemporal evolution of land surface temperature of Lake Oubeira catchment, northeastern Algeria. *Journal of Water and Land Development*, 151-157. doi.org/10.2478/jwld-2019-0073

Shao, C., J. Chen, H. Chu, C. A. Stepien and Z. Ouyang (2020). Intra-Annual and Interannual Dynamics of Evaporation Over Western Lake Erie. *Earth and Space Science* 7(11). doi.org/10.1029/2020EA001091

Sharma, K. V., Kumar, V., Khandelwal, S., & Kaul, N. (2024). Spatial enhancement of Landsat-9 land surface temperature imagery by Fourier transformation-based panchromatic fusion. *International Journal of Image and Data Fusion*, 15(1), 88-109. doi.org/10.1080/19479832.2023.2293077

Siadatmousavi, S. M. and S. A. Seyedalipour (2019). Seasonal Variation of Evaporation from Hypersaline Chemistry, Springer International Publishing: 9-25.

Singh, R., V. Saritha, & C. B. Pande (2024). Monitoring of wetland turbidity using multi-temporal Landsat-8 and Landsat-9 satellite imagery in the Bisalpur wetland, Rajasthan, India." *Environmental Research* 241: 117638. doi.org/10.1016/j.envres.2023.117638

Sugita, M., S. Ogawa and M. Kawade (2020). "Wind as a Main Driver of Spatial Variability of Surface Energy Balance Over a Shallow 102-km2 Scale Lake: Lake Kasumigaura, Japan." *Water Resources Research* 56(8). doi.org/10.1029/2020WR027173

Tasumi, M. (2019). Estimating evapotranspiration using METRIC model and Landsat data for better understandings of regional hydrology in the western Urmia Lake Basin. *Agricultural Water Management* 226: 105805. doi.org/10.1016/j.agwat.2019.105805

Utami, A. N., Kim, T., (2023). Automated Water Surface Extraction in Satellite Images Using a Comprehensive Water Database Collection and Water Index Analysis. *Korean Journal of Remote Sensing*, Vol. 39, No. 4, p. 425–440. doi.org/10.7780/kjrs.2023.39.4.4

Wang, F., Qin, Z., Song, C., Tu, L., Karnieli, A., & Zhao, S., (2015). An improved mono-window algorithm for land surface temperature retrieval from Landsat 8 thermal infrared sensor data. *Remote Sensing*, 7, 4268–4289. doi.org/10.3390/rs70404268

Woolway, R. I., Verburg, P., Lenters, J. D., Merchant, C. J., Hamilton, D. P., Brookes, J., & Jones, I. D. (2018). Geographic and temporal variations in turbulent heat loss from lakes: A global analysis across 45 lakes. *Limnology and Oceanography*, 63(6), 2436-2449. doi.org/10.1002/lno.10950

Zerouali, B., Bailek, N., Bouchouich, K., Mawloud, G., Kuriqi, A., Sami Khafaga, D., & El-kenawy, E. S. M. (2025). Enhancing water security through advanced modeling: integrating deep learning and a novel metaheuristic optimization algorithm for accurate pan evaporation prediction. *AQUA—Water Infrastructure, Ecosystems and Society*, 74(1), 18-35. doi.org/10.2166/aqua.2024.128

Zhang, X., Xu, Y., Han, S., Weng, X., Che, W., Gu, K., & Hou, J. (2025). Development and characterization of novel wood-based composite materials for solar-powered atmospheric water harvesting: A machine intelligence supported approach. *Journal of Cleaner Production*, 497, 145061. doi.org/10.1016/j.jclepro.2025.145061

Zhang, Z., Tang, Q., Zhao, G., Gaffney, P. P., & Dubois, N. (2024). Lake depth, a key parameter regulating evaporation in semi-arid regions: A case study from Dali Lake, China. *Hydrological Processes*, *38*(6), e15196. doi.org/10.1002/hyp.15196

Zhao, G., Li, Y., Zhou, L., & Gao, H. (2022). Evaporative water loss of 1.42 million global lakes. *Nature Communications*, *13*(1), doi.org/10.1038/s41467-022-31125-6

Zhou, W., Wang, L., Li, D., & Leung, L. R. (2021). Spatial pattern of lake evaporation increases under global warming linked to regional hydroclimate change. *Communications Earth & Environment*, *2*(1), 255. doi.org/10.1038/s43247-021-00327-z